Ab-initio density functional theory study of a WO_3 NH_3-sensing mechanism*

Hu Ming(胡 明)†, Zhang Jie(张 洁), Wang Wei-Dan(王巍丹), and Qin Yu-Xiang(秦玉香)

School of Electronics and Information Engineering, Tianjin University, Tianjin 300072, *China*

(Received 6 October 2010; revised manuscript received 13 April 2011)

WO_3 bulk and various surfaces are studied by an *ab-initio* density functional theory technique. The band structures and electronic density states of WO_3 bulk are investigated. The surface energies of different WO_3 surfaces are compared and then the (002) surface with minimum energy is computed for its NH_3 sensing mechanism which explains the results in the experiments. Three adsorption sites are considered. According to the comparisons of the energy and the charge change between before and after adsorption in the optimal adsorption site O_{1c}, the NH_3 sensing mechanism is obtained.

Keywords: WO_3, density functional theory, NH_3 sensing, density of state

PACS: 21.60.De, 21.60.Jz, 31.10.+z **DOI:** 10.1088/1674-1056/20/8/082101

1. Introduction

The detection of gas molecules relevant to chemical and biochemical processes is of critical importance in industrial, environmental and medical monitoring. In practice, solid-state gas sensors are commonly utilized for the monitoring task.[1,2] Semiconducting metal oxide materials have attracted considerable attention during the past decade because of advantages such as their chemical sensing property and great compatibility with microelectromechanical processing.[3−5] Among the metal oxides which change their electrical resistance properties under reaction with surrounding gases, WO_3 was considered as one of the most promising materials for ammonia detection.[6] As a consequence, the understanding of the surface reactions at the solid–gas interface was the object of several studies, aimed to improve the WO_3 electrical response.[7] However, the sensing mechanism was argued based on experimental phenomena.[8] To reveal the mechanism of gas sensors, theoretical calculations are an effective way to model the physical and chemical properties of complex solids at an atomic level as a complement to experimental work. As for WO_3 nanomaterial, there are few reports on WO_3 crystal model computation and surface sensing mechanism; although its sensing properties have been well studied for several years.[9−11] Thus, a theoretical study on WO_3 surface properties is of significance for the development of relevant experiments.

In this paper, a WO_3 bulk model is built and optimized. Then we perform periodic density functional theory total energy calculations to study the energetics of WO_3 surfaces by using the slab model. Considering that the surface with minimal energy is best to crystallize, we investigate the NH_3-sensing mechanism of the surface with the lowest energy.

2. Computational details

2.1. Method

We performed a first-principle calculation based on spin-polarized DFT.[12,13] All calculations were carried out by using the Cambridge sequential total energy package (CASTEP)[14,15] in Materials Studio (Version 4.4) of Accelrys Inc. The widely used local density approximation (LDA) with the exchange correlation functional parameterized by Ceperley and Alder (CA-PZ) was adopted.[16] The cutoff energy of the plane waves was set to be 310 eV. For the surface calculation, the cutoff energy of the plane

*Project supported by the National Natural Science Foundation of China (Grant Nos. 60771019 and 60801018), Tianjin Research Program of Application Foundation and Advanced Technology, China (Grant No. 11JCZDJC15300), Tianjin Natural Science Foundation, China (Grant No. 09JCYBJC01100), and the New Teacher Foundation of Ministry of Education, China (Grant No. 200800561109).

†Corresponding author. E-mail: huming@tju.edu.cn

© 2011 Chinese Physical Society and IOP Publishing Ltd

waves was 340 eV. The Brillouin zone integration was performed using a 3×4×1 Monkhorst–Pack grid. The convergence criteria for structural optimization and energy calculation were set to be medium quality with tolerance for self-consistent field (SCF), energy, maximum force and a maximum displacement of 2.0×10^{-6} eV/atom, 2.0×10^{-5} eV/atom, 0.05 eV/Å, and 2.0×10^{-3} Å (1 Å=0.1 nm), respectively. A Fermi smearing of 0.1 eV was utilized.

2.2. Model

Based on experiment data,[17] WO_3 monoclinic crystal was built and optimized. The surfaces were obtained by cleaving WO_3 crystal and represented by one upper layer with relaxation, while two lower layers were fixed to simulate the bulk layers. In order to reduce the interaction of the close periodical image, the unit cell was doubled with a 15-Å vacuum slab placed on it. Some low-indexed (001), (100), (101), (010), (020), and (002) surfaces were studied; the models of these surface are shown in Fig. 1. The surfaces were simulated within slab geometries and for all orientations the slabs were based on (1×1) geometries. 3×4×1 k-point grids were used. After comparison of the surface energies, we selected the surface with the lowest energy as a model to calculate NH_3 adsorption properties.

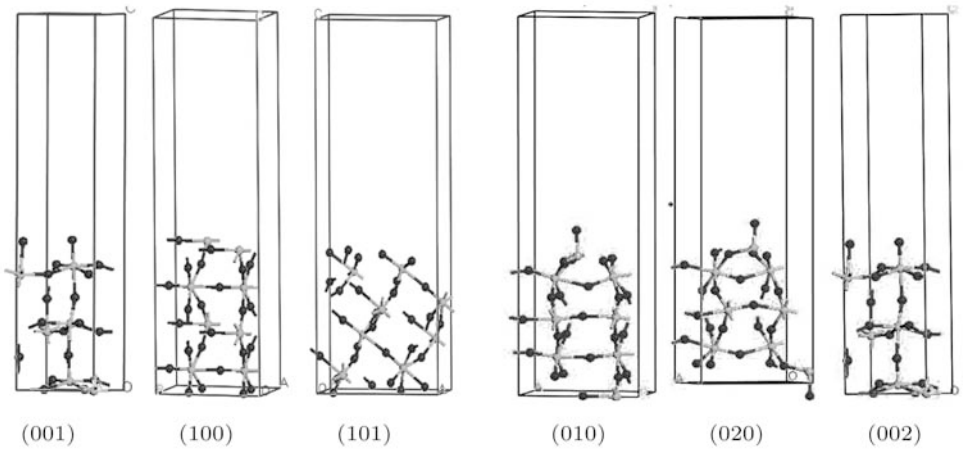


Fig. 1. Low-indexed WO_3 surface models (light balls represent W atoms; dark balls represent O atoms).

For the n-type semiconductor, band gap E_g is defined as[8]

$$E_g = E_c - E_v, \tag{1}$$

where E_c and E_v represent the lowest unoccupied and the highest occupied levels, respectively. As E_F varies between E_c and $(1/2)(E_c + E_v)$ for n-type semiconductors, E_F is considered to be at LDA mid-gap in this paper.

We used the surface energy method to predict the surface energetics of WO_3. The surface energy is calculated from the difference between the total energy in the bulk per unit surface area and the energy of the surface ions[18,19] as shown below

$$E_{surf} = (E_{slab} - nE_{bulk})/A, \tag{2}$$

where E_{surf} is the surface energy, E_{slab} is the total energy per repeated slab supercell, E_{bulk} is the energy per unit cell in the bulk, n is the number of unit cells and A is the total surface area per repeated unit. For a crystal in equilibrium with its surroundings, the surface energy must be minimal for a given volume. Hence the surface morphology has an important effect on surface energy.

3. Results and discussion

3.1. Properties of bulk WO_3

3.1.1. Geometric structure of WO_3

WO_3 crystallizes in the primitive anorthic system with space group $P21/C$. The calculated structural parameters and bond lengths of bulk WO_3 are given in Table 1. It is found that the bulk structures of WO_3 are well reproduced. The calculated result is in good

agreement with the experimental result.[17] The atom periodic arrangement is shown in Fig. 2.

Table 1. Optimized structure parameters of WO_3 bulk.

Lattice parameters/Å	Cell angles/(°)
$a = 5.278604$	$\alpha = 90.000000$
$b = 5.123629$	$\beta = 90.931293$
$c = 7.659448$	$\gamma = 90.000000$

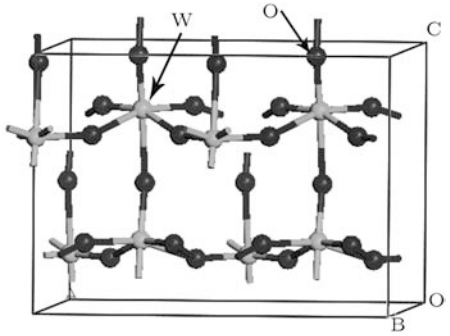


Fig. 2. Model of WO_3 (light balls represent W atoms; dark ones mean O atoms).

3.1.2. Band structure and electronic state of WO_3

The band structure and partial density of states (PDOS) are shown in Figs. 3 and 4.

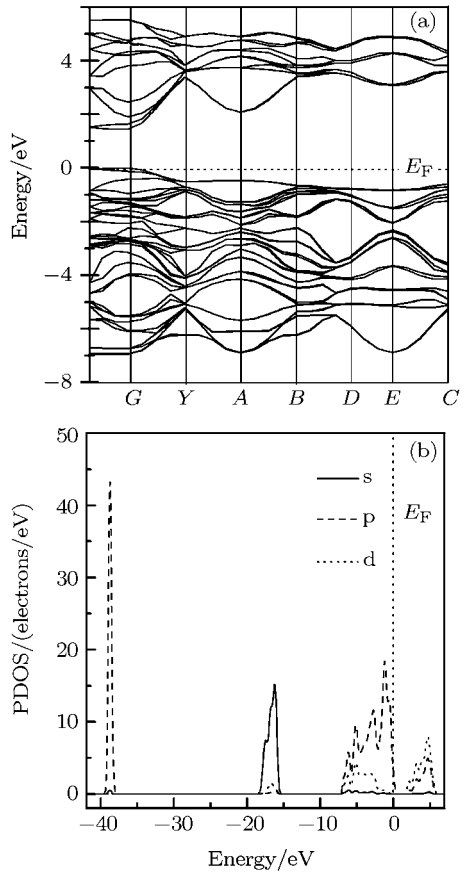


Fig. 3. (a) Band structure and (b) partial density of state (PDOS) of the bulk WO_3.

The total bulk energy was calculated to be −25994.4043 eV, the band gap 1.446 eV and Fermi energy 3.2619 eV. The figure of the band structure also shows that WO_3 is a direct band gap material and the Fermi energy level sites in band gap.[20] Figure 3(b) depicts that the valence band mainly consists of the 2p, 2s states of O and 5d states of W. It can be observed that O 2s states are predominantly found between −18.9 eV∼ −15.0 eV, while the O 2p states appear in a range of −7.5 V ∼ 0.7 eV, which plays a main role for the valance band nearest to Fermi energy. W 5d states give rise to some bands in ranges of −18.5 eV ∼ −15 eV and −7.5 eV ∼ 0.5 eV below the valence band maximum. In addition, the lowest conduction band is dominated by W 2s states, and O 2p and W 5d states have great effects on conductive band above Fermi energy.

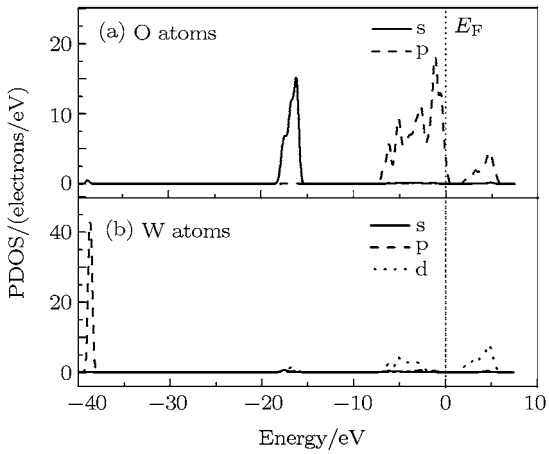


Fig. 4. The PDOS in intrinsic WO_3 of (a) O atoms and (b) W atoms.

3.2. Surface energy of WO_3

The relaxation of the slab surfaces has an apparent effect on surface energy. It makes the surface close to the real surface. It is reported that the surface relaxation reduces the surface energy by as much as 80%. From Table 2, we can see that the WO_3 (002) surface has the lowest energy; while surfaces (101) and (020) have the same highest surface energy. Based on equilibrium morphology theory, the crystal surface energy is related to its growth morphology and it prefers to crystallize towards a low energy state.[21,22] Therefore, we choose a WO_3 (002) surface to study the NH_3 sensing mechanism further.

Table 2. WO_3 surface energies.

WO_3 indexed surface	Surface energy /(eV/Å^2)	Convergence /10^{-7}
(001)	0.2844	3.831
(100)	0.3514	2.035
(101)	0.5863	3.619
(010)	0.3872	2.398
(020)	0.5863	6.184
(002)	0.1738	1.490

3.3. NH_3 adsorption on a WO_3 (002) surface

3.3.1. Adsorption models of NH_3 adsorption on a (002) surface

The ideal (002) surface model is shown in Fig. 5. All of the atoms are arranged in periodic way with three slabs and the outermost oxygen atoms are 1-fold coordinated and defined as O_{1c}; W atoms in plane are 6-folds as W_{6c} and oxygen atoms in plane with 2-fold coordinate are marked as O_{2c}. When building the model of NH_3 adsorption on a (002) surface, we developed three models with the N atom connecting to the surface, considering that it is easier for N to coordinate with O and W atoms.[23,24] In our work, we built three possible models. As shown in Fig. 6, figure 6(a) shows the NH_3 adsorption on O_{1c} site, named S_1; figure 6(b) indicates the model of NH_3 adsorption on W_{6c} site, marked S_2, and figure 6(c) exhibits the model of NH_3 adsorption on O_{2c} site, named S_3.

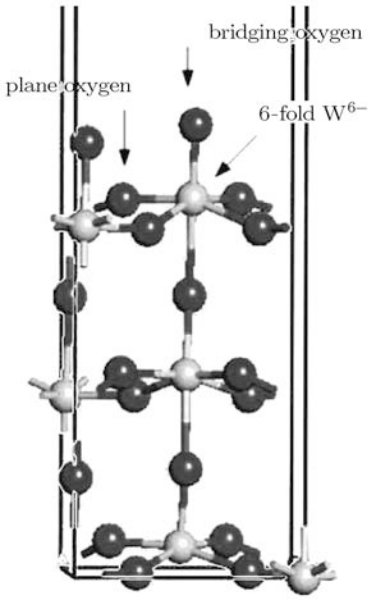


Fig. 5. Ideal WO_3(002) surface model.

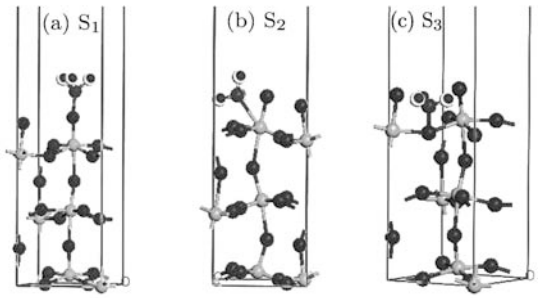


Fig. 6. NH_3 adsorption models on (002) surface.

3.3.2. Optimum adsorption site of NH_3

In order to investigate the adsorption site of NH_3, the adsorption energies of different models were calculated first. Table 3 shows the results of adsorption energies for different adsorption models. It is obvious that NH_3's were adsorbed on three sites spontaneously without any extra energy (all adsorption energies are negative). In terms of energy, the S_1 model is the most stable and probable adsorption structure. It is also reasonable because O_{1c} has a free bond and is also the topmost atom. Thus, next we will discuss the adsorption properties of NH_3 on (002) surface O_{1c} adsorption, specifically.

The whole system was first optimized in order to calculate its physical properties. Then through the difference between the reconstructed surface and the whole system, the adsorption energy and contribution from charge transfer were gained. The adsorption energy can be expressed as[25−27]

$$E_{\text{ads}} = E_{\text{NH3+surf}} - E_{\text{surf}} - E_{\text{NH3}}, \tag{3}$$

where $E_{\text{NH3+surf}}$ is the total energy for the slab with adsorbed NH_3 on the surface; E_{surf} and E_{NH3} represent the total energy of surface and free NH_3 molecular, respectively.

Table 3. Adsorption energies of different models.

Calculated model	WO_3 (002)	NH_3	S_1	S_2	S_3
Energy/eV	–19486.542	–319.490	–19811.639	–19811.552	–19810.709
Adsorption energy/eV			–5.607	–5.520	–4.677

When the WO_3 (002) surface is exposed to gas atmosphere, we distinguish two sensing mechanisms:

(i) adsorption-induced reconstruction of the WO_3 surface, which occurs as the adsorbate approaches. The band structure changes correspondingly with the change of adsorbate type and E_b;

(ii) charge transfer, which occurs because of the relation between electron affinity of adsorbate and the work function of the WO_3 surface.

These two mechanisms both contribute to the charge redistribution in the WO_3 surface and the change of E_g correspondingly. As intrinsic conductivity is controlled by $\exp(-E_g/K_BT)$ under a certain temperature, a change of electronic conductance can be observed in experiment. In the following, we discuss NH_3 molecule adsorption on a (002) WO_3 surface.

3.3.3. Effect of NH_3 adsorption on a WO_3 (002) surface O_{1c} site on surface structure

The geometrical structure of NH_3 on (002) surface O_{1c} adsorption is that N atom reacts with O_{1c} vertically; the bond length of N–O_{1c} is 1.40092 Å; the bond lengths of N–H change a lot as shown in Table 4.

Table 4. Bond lengths of N–H/Å.

Bond length	Before adsorption	After adsorption
N–H_1	1.02793	1.03583
N–H_2	1.02911	1.85994
N–H_3	1.02840	1.05348

Table 5 shows the relative displacements of the WO_3 (002) surface outermost atoms after NH_3 adsorption. Except for two-fold O_{2c} swelling outside, other kinds of ions all move towards the internal part of the structure. This indicates that NH_3 adsorption does not change the surface structure clearly. Because NH_3 complements the free bond on the surface, the surface relaxation phenomenon is changed.

Table 5. Relative displacements of the outermost atoms after NH_3 adsorption.

Model	Relative displacement/nm		
	O_{1c}	W_{6c}	O_{2c}
(002) surface	–0.2615	–1.9250	–2.5745
NH_3 adsorbed on (002) surface	–0.2958	–2.1879	–2.4490

3.3.4. Effect of the NH_3 adsorption on the surface of the O_{1c} site on surface conductive property

Comparing the DOS/PDOS figures of the WO_3 (002) surface before and after NH_3 adsorption, as shown in Figs. 7 and 8, we can find that the adsorption has had a certain influence on the DOS of the whole surface. As for the lower valence band between −42 eV∼ −35 eV, the band width and peak number both decrease after adsorption, which are caused mainly by the W 5p states, as shown by comparing Fig. 7 with Fig. 4; while for upper valance band in a range of −25 eV∼ 0.7 eV, the curve shape changes a lot, especially the peak number is reduced and the topmost peak moves from −4.59 eV to −5.45 eV, which are apparently induced by the change of O 2s and 2p states as shown by comparing Fig. 7 with Fig. 8. At the Fermi level, the whole electronic state drops off by about 6.5 electrons/eV, from 15.5 electrons/eV down to 9.0 electrons/eV. Above the Fermi level, the peak increases by almost 4 electron/eV. From Fig. 8 it follows that the changes in electronic state near the Fermi level are due mainly to the changes of O 2s and 2p states.

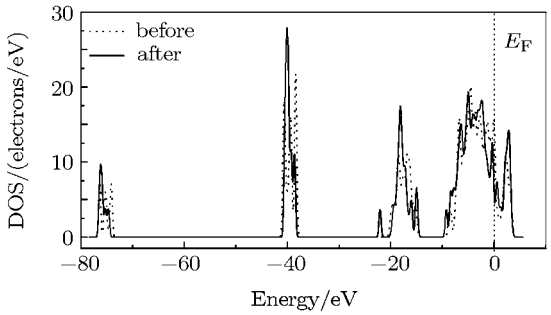


Fig. 7. DOSs of WO_3 (002) surface before and after NH_3 adsorption.

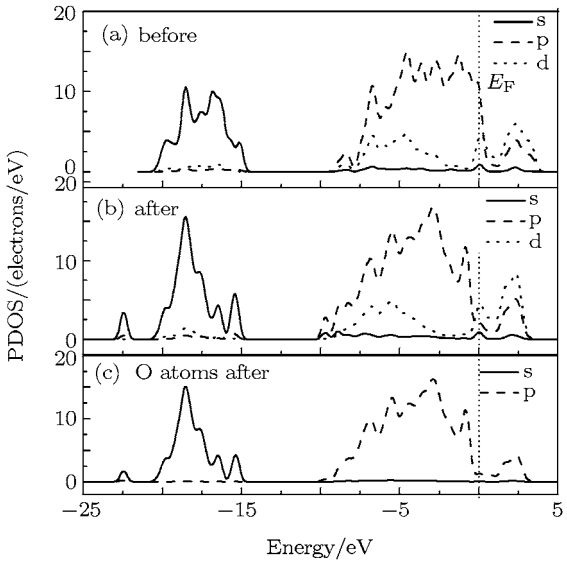


Fig. 8. PDOSs of WO_3 (002) surface: (a) before and (b) after NH_3 adsorption, and (c) PDOS of O atoms after NH_3 adsorption.

The PDOSs in Figs. 9(a) and 9(b) show that O_{1c} 2p states at the Fermi level drop off from 4.2 electrons/eV to zero after adsorption. Obviously, a new peak appears in a range of -10 eV~ -7 eV, which makes the band range widen from -10 eV to -0.5 eV. Although the peak number increases, the heights of all peaks decrease a lot, by almost a half. These are the consequence of O_{1c}–N bond interaction. Thus, the O_{1c} 2p state contributes to the whole DOS change. Also, because the peak height decreases, it appears as a less sharp peak in the whole DOS. It should also be noticed that the O_{1c} 2s state appears at about -16 eV after adsorption, which is consistent with the total DOS.

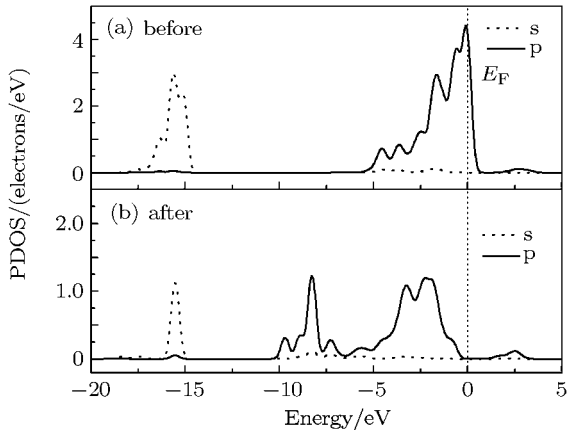


Fig. 9. PDOSs of O_{1c} before (a) and after (b) NH_3 adsorption on surface.

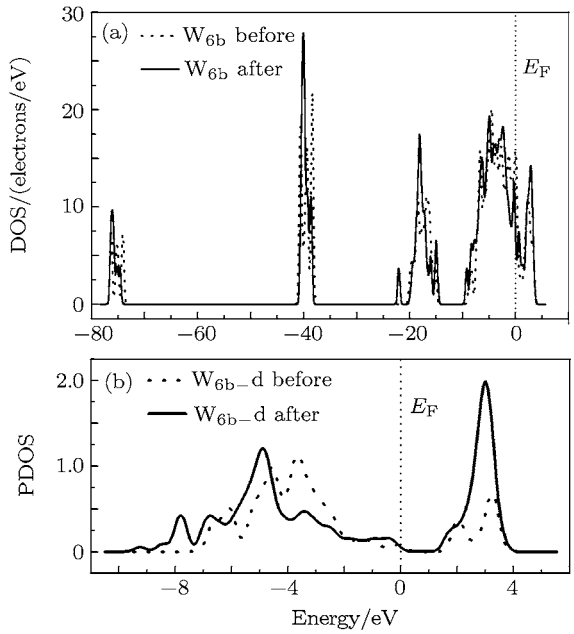


Fig. 10. (a) DOSs of W_{6b} and (b) PDOSs of W_{6b} 5d states before and after NH_3 adsorption on surface.

From Fig. 10 (a), it can be seen that there are few changes of the states, except for all states shifting toward the left after adsorption. Owing to the change of W_{6b} 5d state clearly seen from Fig. 10(b), the peak in the conductive band rises to about 1.2 electrons/eV, which is the cause of conductive band peak rise in the whole DOS.

From Figs. 11(a) and 11(b), it is obvious that after adsorption, the band width is narrower, while the heights of all peaks sharply fall to one-tenth of those before. At the same time, the peak number is also reduced. The O_{2c} 2p state peak above the Fermi level drops off by about 3 electrons/eV. All of these changes correspond to the total DOS change.

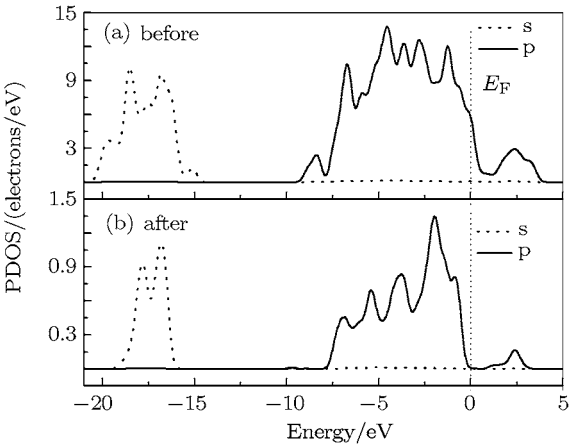


Fig. 11. PDOSs of O_{2c} (a) before and (b) after NH_3 adsorption on surface.

From all the analyses stated above, NH_3 adsorption not only affects the O_{1c} atom state density on adsorbing site O_{1c}, but also exerts a certain influence on other atoms at the surface. Except for the above PDOS change, adsorption does not add an extra state to the band gap; but NH_3 adsorption makes the Fermi energy change from -2.2701 eV to -1.1943 eV, which means that the surface density state shifts toward the right by about 1.08 eV in total. Therefore, both DOS change and Fermi energy increase are the main reasons for the change of surface conductive properties.

3.3.5. Electron population analysis of NH_3 adsorption on (002) surface O_{1c} site

Table 6 shows that electron populations of a NH_3 molecule before and after adsorption on an O_{1c} site. After adsorption, for the N atom, 2s and 2p electrons both decrease, for the H atom of H_3, some 1s electrons are lost, while for other H atoms of, for example, H_1 and H_2, 1s electrons increase. So the bond energy of N–H changes, which can also be indicated by the bond length change.

The free NH_3 molecules before adsorption are of electric neutrality, while after adsorption, the electron number of N atom reduces 0.65, the number of the H atom increases 0.03, thus the electron number of the whole NH_3 molecule is reduced by 0.62. As for the (002) WO_3 surface, it will obtain 0.62 electron transfer from the NH_3 molecule; so the resistance of the surface decreases. This result is in good agreement with the experimental result. The electron population provides the number of transferred electrons resulting from adsorption, quantitatively.

Table 6. Electron populations of NH_3 molecule before and after adsorption.

Atom	Before adsorption/e			After adsorption/e		
	s	p	Total	s	p	Total
H_1	0.57	0.00	0.57	0.63	0.00	0.63
H_2	0.57	0.00	0.57	0.58	0.00	0.58
H_3	0.57	0.00	0.57	0.53	0.00	0.53
N	1.76	4.53	6.30	1.65	4.00	5.65

4. Comparison with existing experiments

WO_3 nano-thin films (0.9 cm×2.4 cm) were deposited on porous silicon substrates at room temperature (RT) by a DPS-III ultra-high vacuum facing target magnetron sputtering system. The sensors were fabricated as follows:[28] two interdigital Pt electrodes were deposited on the top surface of WO_3 film. The structure of the sensor is given in Fig. 12. After annealing at 450 °C in dry air for 4 h, the sensors were loaded into a homemade static gas test system and connected to outside electronics to monitor their resistance change independently. The sensor response is defined as

$$S = (R_{\rm gas} - R_{\rm air})/R_{\rm air}, \tag{4}$$

where $R_{\rm air}$ is the resistance in ambient air and $R_{\rm gas}$ is the maximum resistance in NH_3 and air-mixed gas.

Figure 13 shows the response and the recovery of WO_3/PS gas sensor upon exposure to 50-ppm NH_3 at room temperature 20 °C and 50 °C, respectively. When the target gas was injected into the chamber, the sensor showed an obvious decrease of resistance. This phenomenon can be explained by our theoretical computational results. First of all, $E_{\rm F}$ improvement after NH_3 adsorption makes the carriers move to conductive band easily, so that the resistance is reduced. In addition, NH_3 molecules injection brings some electrons into WO_3 surface; WO_3 is an n-type semiconductor, so the increase of electron number causes the number of carriers to increase. This is another factor used for reducing resistance.

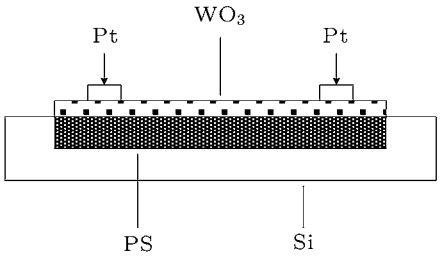


Fig. 12. Schematic diagram of WO_3/PS gas sensor.

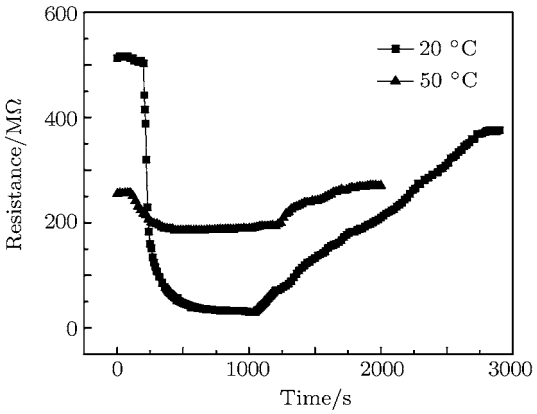


Fig. 13. Response and recovery of WO_3/PS to 50-ppm NH_3 at 20 °C and 50 °C.

5. Conclusion

In this paper, DFT calculations are performed to reveal WO_3 crystal and surface properties. WO_3 is a direct band gap material and the band gap is 1.446 eV. After energy calculation of several low index surfaces, a WO_3 (002) surface with the lowest surface energy, 0.1738 eV, appears to have the most stable electronic structure.

The (002) surface is examined for a NH_3 gas-sensing mechanism because of its advantages of electronic stability and low energy. In terms of energy, the adsorption way in which NH_3 connects to O_{1c} atom of (002) surface with N atom is the most stable. NH_3 adsorption does not change the surface structure clearly. Because NH_3 complements the free bond on the surface, the surface relaxation phenomenon is changed. Adsorption does not add any extra state to the band gap; but NH_3 adsorption makes the Fermi energy change from −2.2701 eV to −1.1943 eV; and the surface density state moves toward the right by about 1.08 eV wholly. At the same time, (002) surface obtains 0.35 electrons transferred from NH_3 molecule.

Based on the above analyses, two mechanisms control this sensing process—the adsorption-induced

reconstruction of the WO_3 surface and the charge transfer leading to changes of the electronic structure of the (002) WO_3 surface, resulting in a change of resistance. When the NH_3 molecule is adsorbed on the surface, the resistance of the gas sensor changes because of the joint effect of these two mechanisms. These results are shown to be in good accordance with our experimental results and conducible to the understanding of the sensing mechanism of WO_3-based gas sensors.

References

[1] An W, Wu X J and Zeng X C 2008 *J. Phys. Chem.* C **112** 5747

[2] Ma H L, Fan D W and Niu X S 2010 *Chin. Phys.* B **19** 076102

[3] Hu X L, Li G S and Yu J C 2010 *Am. Chem. Soc.* **26** 3031

[4] Chen L Y, He Z S, Yan T, Bai S L, Chen A F and Liu C C 2005 *Progress in Natural Science* **15** 669

[5] Dai C L and Liu M C 2007 *Jpn. J. Appl. Phys.* **46** 843

[6] Liu Z F, Yamazaki T, Shen Y B, Kikuta T and Nakatani N 2007 *Sensors and Actuator* B **128** 173

[7] Morazzoni F, Scotti R, Origoni L, D'Arienzo M, Jimenez I, Cornet A and Morante J R 2007 *Catalysis Today* **126** 169

[8] Yuan Q Z, Zhao Y P, Li L M and Wang T H 2009 *J. Phys. Chem.* C **113** 6107

[9] Levy M and Pagnier T 2007 *Sensors and Actuators* B **126** 204

[10] Bittencourt C, Felten A, Espinosa E H, Ionescu R, Llobet E, Correig X and Pireaux J J 2006 *Sensors and Actuators* B **115** 33

[11] Xie G Z, Yu J S, Chen X and Jiang Y D 2007 *Sensors and Actuators* B **123** 909

[12] Hohenberg P and Kohn W 1964 *J. Phys. Rev.* B **136** 864

[13] Kohn W and Sham L J 1965 *J. Phys. Rev.* **140** A1133

[14] Payne M C, Teter M P, Allan D C, Arias T A and Joannopoulos J D 1992 *Rev. Mod. Phys.* **64** 1045.

[15] Milman V, Winkler B, White J A, Pickard C J, Payne M C, Akhmataskaya E V and Nobes R H 2000 *J. Quantum Chem.* **77** 895

[16] Kotochigova S, Levine Z H, Shirley E L, Stiles M D and Clark W C 1997 *Phys. Rev.* A **55** 191

[17] Udachin K A, Ratcliffe C I and Ripmeester J A 2002 *J. Supramolecular Chemistry* **2** 405

[18] Casassa S and Pisani C 1995 *Phys. Rev.* B **51** 7805

[19] Polatoglou H M, Methfessel M and Scheffler M 1993 *Phys. Rev.* B **48** 1877

[20] Jiang X S, Yan Y C, Yuan S M, Mi S, Niu Z G and Liang J Q 2010 *Chin. Phys.* B **19** 107104

[21] Xu X L, Chen Z H, Li Y, Chen W K and Li J Q 2009 *Surf. Sci.* **603** 653

[22] Bentmann H, Demkov A A, Gregory R, and Zollner S 2008 *Phys. Rev.* B **78** 205302-1

[23] Ma S Y and Wang S Q 2008 *Chin. Phys.* B **17** 3856

[24] Ying M J, Zhang P and Du X L 2009 *Chin. Phys.* B **18** 275

[25] Xue Y B, Tang Z A and Wei G F 2007 *Chinese Journal of Sensors and Actuators* **20** 2364 (in Chinese)

[26] Yang Y 2010 *Chin. Phys.* B **19** 108201

[27] Xue Y B and Tang Z A 2009 *Chem. J. Chin. University* **30** 583 (in Chinese)

[28] Sun F Y, Hu M, Sun P, Zhang J and Liu B 2010 *Journal of Nanoscience and Nanotechnology* **10** 7739